

Interlayer Heat Transfer in Bilayer Carrier Systems

Mika Prunnila* and Sampo J. Laakso

VTT Technical Research Centre of Finland, P.O.Box 1208, FIN-02044 VTT, Espoo, Finland

(Dated: August 28, 2021)

We study theoretically how energy and heat are transferred between the two-dimensional layers of bilayer carrier systems due to near-field interlayer carrier interaction. We derive general expressions for the interlayer heat transfer and thermal conductance. Approximation formulas and detailed calculations for semiconductor and graphene based bilayers are presented. Our calculations for GaAs, Si and graphene bilayers show that the interlayer heat transfer can exceed the electron-phonon heat transfer below (system dependent) finite crossover temperature. We show that disorder strongly enhances the interlayer heat transport and pushes the threshold towards higher temperatures.

PACS numbers: 72.20.-i, 73.50.-h

I. INTRODUCTION

Interlayer momentum transfer (the drag effect) has been extensively investigated in bilayer carrier systems, where two two-dimensional (2D) carrier gases are separated by a thin barrier. The drag effect is a manifestation of near-field interlayer interaction and bilayer carrier systems provide a unique laboratory for probing charge carrier interactions and interaction driven phases (see Refs. [1, 2] for a review). Since the pioneering experiment of electron-electron drag between two coupled 2D electron gas (2DEG) layers in GaAs-AlGaAs heterostructure [3] 2D carrier bilayers have been demonstrated in variety of semiconductor structures. Recently, the drag effect has been experimentally investigated also in graphene bilayer, where two single layer graphene flakes are separated by a dielectric.[4]

The investigations of bilayer carrier systems have been focused on the drag phenomenon, but the interlayer interaction also mediates energy and heat transfer between the layers (see Fig. 1) and such near-field energy/heat transfer is the topic of the present Paper. Considerable efforts have been devoted to understand near-field heat transfer via different channels between bodies that are separated by a small vacuum gap.[5–7] One of the most significant heat exchange channels is built from inter-body photon coupling. Surface excitations involving optical phonons and plasmons can play an important role and these so-called polariton effects can strongly enhance the near-field

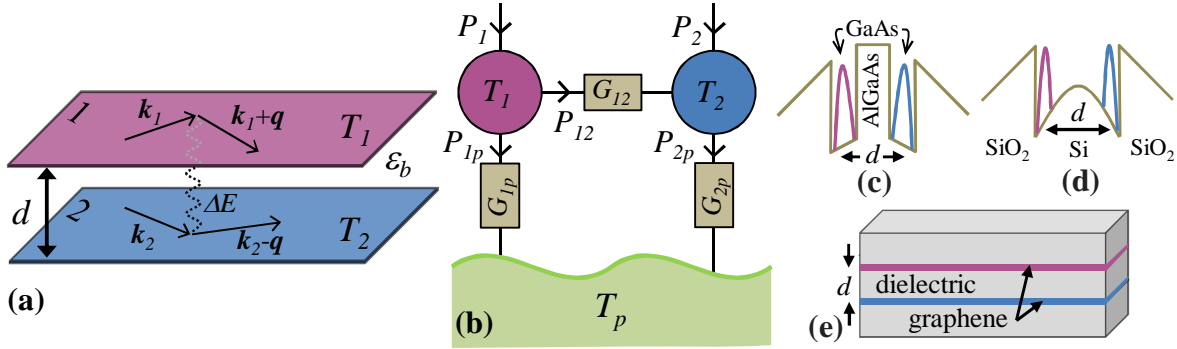


FIG. 1. (color online) (a) Illustration of near-field scattering processes (momentum and energy transfer) between 2D carrier layers 1 and 2 separated by a distance d and embedded in a solid with dielectric constant ϵ_b . The layers are at local temperatures T_1 and T_2 . A carrier in layer 1 (2) experiences momentum scattering $\mathbf{k}_1 \rightarrow \mathbf{k}_1 + \mathbf{q}$ ($\mathbf{k}_2 \rightarrow \mathbf{k}_2 - \mathbf{q}$) due to interlayer interaction. During the process energy ΔE is transferred between the layers. (b) The equivalent thermal circuit. P_L is the input heating/cooling power ($L = 1, 2$) and G_{12} is the interlayer thermal conductance. Due to the interlayer scattering processes $G_{12} \neq 0$ and power (or heat) P_{12} flows between the layers. Layers couple to phonon bath, which is at temperature T_p , via electron-phonon thermal conductance G_{Lp} and power P_{Lp} flows to the bath. Illustration of conduction band diagram and electron wavefunctions of (c) GaAs and (d) Si bilayer. (e) Graphene bilayer with dielectric barrier.

* mika.prunnila@vtt.fi

energy transfer.[6] Recently, a near-field heat transfer channel arising directly from lattice vibrations has also been proposed.[8, 9] Near-field heat transfer is naturally always present between closely spaced systems, even in the case of solid contact, but then the effect is expected to be strongly masked by competing heat dissipation channels formed by solid heat conduction and/or electron-phonon coupling. One of the motivation for the present work is to challenge this line of thought and, indeed, by detailed calculations we will show that in bilayer carrier systems the near-field heat transfer can become the dominant interlayer heat transfer mechanism.

In this work, we derive general expression of charge fluctuation induced interlayer energy transfer rate, which is applicable to semiconductor and graphene bilayers. In the derivation we use perturbation theory and fluctuation-dissipation relations. Our formula for the interlayer thermal conductance, G_{12} , has strong connection to the drag resistance formulas[10]. The interlayer thermal conductance is intimately connected to fluctuations and dissipative properties of the individual layers. This is explicitly seen as the presence of the imaginary parts of the layer susceptibilities in the G_{12} formula and it is a manifestation of fluctuation-dissipation theorem. Approximation formulas and detailed calculations of G_{12} in the case of screened Coulomb interlayer interaction are presented and we show that interlayer thermal transport is strongly enhanced due to disorder. As the layers are in the same solid there exist competing energy relaxation channels. At the temperatures of interest electron-phonon coupling to the bulk thermal phonons is the relevant competing heat dissipation mechanism [see Fig. 1(b)]. It is shown that remarkably G_{12} can dominate over the electron-phonon coupling. Therefore, near-field heat transfer can become a dominant heat transfer mechanism even in the case of solid contact.

II. THEORY

In this Section we derive general expression for the interlayer thermal conductance G_{12} . Then we introduce approximation formulas for G_{12} and on the basis of the existing literature discuss electron-phonon coupling, which is the competing dissipation channel.

A. Interlayer thermal conductance

The scattering events depicted in Fig. 1(a) are mediated by interlayer interaction which is described by matrix element $M_{\mathbf{q}}$ (to be defined later). The interlayer Hamiltonian H is given by

$$H = \frac{1}{2A} \sum_{\mathbf{q}} M_{\mathbf{q}} \rho_{1\mathbf{q}}^{\dagger} \rho_{2\mathbf{q}}, \quad (1a)$$

$$\rho_{L\mathbf{q}} = \sum_{\mathbf{k}} \sum_{\sigma, \sigma'} \sum_{s, s'} c_{\mathbf{k}-\mathbf{q}, s' \sigma'}^{\dagger} F_{\mathbf{k}-\mathbf{q}, s'}^{\dagger} F_{\mathbf{k}, s} c_{\mathbf{k}, s \sigma}, \quad (1b)$$

where A is the area, $\rho_{L\mathbf{q}}$ is the electron density operator for layer $L = 1, 2$ and $c_{\mathbf{k}, s \sigma}^{(\dagger)}$ is the electron annihilation (creation) operator. Variables \mathbf{k} , s and σ are wavevector, band index and spin index, respectively (here we will assume spin degeneracy). All electron variables depend on the layer index L , but this is typically not written explicitly (e.g. $\mathbf{k} = \mathbf{k}_L$). Factor $F_{\mathbf{k}, s}$ is defined by the wavefunction of the single particle states and product $F_{\mathbf{k}-\mathbf{q}, s'}^{\dagger} F_{\mathbf{k}, s}$ defines a band form factor. For an ideal 2D electron gas (2DEG) we have $F_{\mathbf{k}, s} = 1$ and summation over band indices s, s' can be ignored. For graphene we have $F_{\mathbf{k}, s} = \frac{1}{\sqrt{2}} (1 \quad s e^{i\theta_{\mathbf{k}}})^{\dagger}$, where $s = +1$ and $s = -1$ denote conduction and valence bands, respectively, and $\theta_{\mathbf{k}} = \arctan(k_y/k_x)$.

Next, H will be considered as a perturbation Hamiltonian that will cause transitions from initial state $|i1, i2\rangle = |i1\rangle |i2\rangle$ with energy $E_i = E_{1i} + E_{2i}$ to final state $|f1, f2\rangle = |f1\rangle |f2\rangle$ with energy $E_f = E_{1f} + E_{2f}$. Here $|iL\rangle$ ($|fL\rangle$) is the initial (final) state of layer L . The transition rate Γ_{fi} from initial state i to final state f is given by the golden rule formula

$$\Gamma_{fi} = \frac{2\pi}{\hbar} |\langle f2, f1 | H | i1, i2 \rangle|^2 \delta(E_i - E_f). \quad (2)$$

By multiplying Γ_{fi} by the energy change $\Delta E_1 = E_{1i} - E_{1f}$ and performing an ensemble average over the initial electronic states, and summing over final electronic states we obtain energy transfer rate (heat transfer)

$$P_{12} = \frac{2\pi}{\hbar} \frac{1}{2A} \sum_{\mathbf{q}} \sum_{i1, f1} \sum_{i2, f2} \Delta E_1 \hat{w}_{i1} \hat{w}_{i2} |M_{\mathbf{q}}|^2 \left| \langle f1 | \rho_{1\mathbf{q}}^{\dagger} | i1 \rangle \right|^2 \left| \langle f2 | \rho_{2\mathbf{q}} | i2 \rangle \right|^2 \delta(E_{1i} + E_{2i} - E_{1f} - E_{2f}), \quad (3)$$

where \widehat{w}_{Li} is the weighting factor of carrier layer L in state i . We assume that each layer L can be described by a local temperature T_L and, therefore, $\widehat{w}_{Lf} = \widehat{w}_{Li} \exp[(E_i - E_f)/k_B T_L]$. By using the identity $\delta(E_A + E_B) = \hbar \int_{-\infty}^{+\infty} d\omega \delta(E_A - \hbar\omega) \delta(E_B + \hbar\omega)$ and definition of correlator

$$C_L(\mathbf{q}, \omega) = 2\pi\hbar \sum_{n,m} \widehat{w}_{Ln} |\langle nL | \rho_{L\mathbf{q}} | mL \rangle|^2 \delta(E_{Ln} - E_{Lm} + \hbar\omega) \quad (4)$$

we find

$$P_{12} = \frac{1}{2\pi\hbar^2} \left(\frac{1}{2A} \right)^2 \int_{-\infty}^{+\infty} d\omega \sum_{\mathbf{q}} \hbar\omega |M_{\mathbf{q}}|^2 C_1(\mathbf{q}, -\omega) e^{\hbar\omega/k_B T_2} C_2(\mathbf{q}, -\omega). \quad (5)$$

As we assume internal equilibrium for the different layers we can adopt the fluctuation-dissipation relation [11] $(1 - e^{-\hbar\omega/k_B T_L})C_L(\mathbf{q}, \omega) = -2\hbar A \text{Im}\{\chi_L(\mathbf{q}, \omega)\}$, where $\chi_L(\mathbf{q}, \omega)$ is the susceptibility, which can depend on T_L . Using the fluctuation-dissipation relation and the property $C_L(\mathbf{q}, -\omega) = e^{-\hbar\omega/k_B T_L} C_L(\mathbf{q}, \omega)$ we find the general expression for the interlayer heat transfer

$$P_{12} = \int_0^{+\infty} \frac{d\omega}{2\pi} \sum_{\mathbf{q}} \hbar\omega |M_{\mathbf{q}}|^2 \text{Im}\{\chi_1(\mathbf{q}, \omega)\} \text{Im}\{\chi_2(\mathbf{q}, \omega)\} [n_1(\hbar\omega) - n_2(\hbar\omega)], \quad (6)$$

where $n_L(\hbar\omega) = (\exp(\hbar\omega/k_B T_L) - 1)^{-1}$. At the limit $T_1, T_2 \rightarrow T$ it is useful to define the interlayer thermal conductance $G_{12}(T) = P_{12}/(T_1 - T_2)$. From Eq. (6) we find

$$G_{12}(T) = \frac{1}{4k_B T^2} \int_0^{+\infty} \frac{d\omega}{2\pi} \sum_{\mathbf{q}} (\hbar\omega)^2 |M_{\mathbf{q}}|^2 \frac{\text{Im}\{\chi_1(\mathbf{q}, \omega)\} \text{Im}\{\chi_2(\mathbf{q}, \omega)\}}{\sinh^2(\hbar\omega/2k_B T)}, \quad (7)$$

which has a striking similarity with the bilayer drag resistance formula.[10] Equation (7) has only single temperature and, therefore, it is more convenient to adopt in the case studies instead of Eq. (6).

In the following we will assume that the interlayer interaction is mediated by screened Coulomb interaction, when the matrix element is given by $M_{\mathbf{q}} = \epsilon_{12}^{-1}(\mathbf{q}, \omega) U(\mathbf{q}) F_{12}(d)$, where $U(\mathbf{q}) = e^2/2\epsilon_b q$ is the 2D Fourier transform of Coulomb potential (ϵ_b is the background dielectric constant) and $F_{12}(d)$ is the spatial form factor, which depends on the spatial extent of the electron wave functions and layer distance d . For graphene the extend is practically zero and for the sake of simplicity here we assume vanishing extent for the semiconductor systems as well. Thus, we use $F_{12}(d) = \exp(-qd)$. The inter-layer dielectric function $\epsilon_{12}(\mathbf{q}, \omega)$ is given by $\epsilon_{12}(\mathbf{q}, \omega) = [1 - U(\mathbf{q})\chi_1(\mathbf{q}, \omega)][1 - U(\mathbf{q})\chi_2(\mathbf{q}, \omega)] - F_{12}^2 U(\mathbf{q})^2 \chi_1(\mathbf{q}, \omega)\chi_2(\mathbf{q}, \omega)$. [1, 10]

In the ballistic limit the carrier mean free path l_e exceeds the layer distance ($l_e \gg d$) and we use the ideal 2D susceptibilities. For 2DEG we have [12]

$$\chi_L(\mathbf{q}, \omega) = \nu(2z)^{-1} [2z - \Omega_-(z, u) - \Omega_+(z, u) + F_-(z, u) - F_+(z, u)], \quad (8)$$

where $\Omega_{\pm}(z, u) = C_{\pm} \sqrt{(z \pm u)^2 - 1}$, $F_{\pm}(z, u) = iD_{\pm} \sqrt{1 - (z \pm u)^2}$, $z = q/2k_F$, $u = \omega/qv_F$, $C_{\pm} = (z \pm u)/|z \pm u|$ and $D_{\pm} = 0$ for $|z \pm u| > 1$, and $C_{\pm} = 0$ and $D_{\pm} = 1$ for $|z \pm u| < 1$. Here v_F (k_F) is the Fermi velocity (wave vector) and $\nu = \nu(\epsilon_F)$ is the density of states at Fermi level $\epsilon_F \gg k_B T$. For ballistic graphene the expression for $\chi_L(\mathbf{q}, \omega)$ is quite lengthy and will not be presented here. It can be found, for example, from Ref. [13].

B. Approximation formulas

Even though there are some fundamental differences between graphene and 2DEGs, the response of these systems is similar at low frequencies and small q . Indeed, for the Taylor series expansion of 2DEG [Eq. (8)] and graphene susceptibilities [13] we find the same result

$$\chi_L(\mathbf{q}, \omega) \simeq -\nu \left(1 + i \frac{\omega}{v_F q} \right). \quad (9)$$

Respectively, in the diffusive limit ($\omega\tau, l_e/d \ll 1$) the susceptibility can be approximated as

$$\chi_L(\mathbf{q}, \omega) \simeq -\nu \frac{iDq^2}{\omega + iDq^2}, \quad (10)$$

where $D = v_F^2 \tau / 2$ is the diffusion coefficient and $\tau = l_e / v_F$ is the momentum relaxation time.

By using Eq. (9) in Eq. (7) for two similar ballistic 2DEG and graphene layers we find asymptotic low-temperature result

$$G_{12}(T) \simeq \frac{f(\kappa d)}{2d^{2-\alpha}} \frac{\hbar}{v_F^\alpha} \left(\frac{k_B}{\hbar} \right)^{2+\alpha} T^{1+\alpha}, \quad (11)$$

where $\alpha = 1.9$, $\kappa = \frac{\nu e^2}{2\varepsilon_b}$ is the screening wave vector and $f(a) \simeq (a^{-2} + 2.21a + 1.24)^{-1}$. The above Equation provides a good approximation when $k_F d k_B T < 2E_F$. Note that parameter κd characterizes the screening of the interlayer interaction: large (small) κd means strong (weak) screening.

In the diffusive limit we use Eq. (10) in Eq. (7) and we find low temperature approximation formula

$$G_{12}(T) \simeq \frac{3A_3}{16\pi} \frac{\varepsilon_b}{d} \frac{1}{2\sigma} \hbar \left(\frac{k_B}{\hbar} \right)^3 T^2. \quad (12)$$

Here $\sigma = e^2 \nu D$ is the DC conductivity of single layer and $A_n = \Gamma(n) \zeta(n) = \int dx x^{n-1} / [\exp(x) - 1]$. Equation (12) is applicable when $(l_e / v_F) k_B T / \hbar < (l_e / d)^2$. Note that the diffusive G_{12} [Eq. (12)] greatly exceeds the one in the ballistic case [Eq. (11)], which is the manifestation of enhanced fluctuations and dissipation due to disorder.

C. Electron-phonon coupling

As depicted in the thermal circuit of Fig. 1(b) G_{12} competes with the electron-phonon thermal conductance G_{Lp} , which at the limit $T_L, T_p \rightarrow T$ is given by $G_{Lp}(T) = P_{Lp} / (T_L - T_p)$. In 2DEGs at low temperatures the electron-phonon energy transfer is dominated by screened deformation potential (G_{Lp}^{DP}) and piezoelectric (G_{Lp}^{PE}) interaction with total thermal conductance $G_{Lp}(T) = G_{Lp}^{DP}(T) + G_{Lp}^{PE}(T)$. For the deformation potential contribution we have [14, 15]

$$G_{Lp}^{DP}(T) = \sum_{\lambda} \frac{F_{6-n} 2^n}{l_e^n \kappa^2} \langle f_n(\theta) \Xi^2 \rangle v_{\lambda}^{n-6} T^{6-n}, \quad (13)$$

where $n = 0(1)$ represents ballistic (diffusive) limit of electron-phonon coupling, for which we have $q_{\lambda T} l_e > 1 (< 1)$. Here $q_{\lambda T} = k_B T / \hbar v_{\lambda}$ is the thermal phonon wave vector, factor $F_i = \frac{\nu A_i}{2\pi^2 \rho v_F} \frac{(i+1)k_B^{i+1}}{\hbar^i}$, $v_L(T)$ is the longitudinal (transversal) phonon velocity and ρ is the mass density of the crystal. The brackets $\langle \dots \rangle$ stand for solid angle average and θ is the angle with respect to the z-axis, which is perpendicular to the layer plane. $\langle f_n(\theta) \Xi^2 \rangle$ is an effective deformation potential coupling and $f_0(\theta) = \sin \theta$ and $f_1(\theta) = \frac{\sin^2 \theta}{\alpha + \sin^2 \theta}$. Parameter $\alpha = (\kappa l_e v_F / v_{\lambda})^{-2}$ and as a result $f_1(\theta) \approx 1$. The piezoelectric coupling gives rise to contribution [14–16]

$$G_{Lp}^{PE}(T) = \sum_{\lambda} \frac{F_{4-n} 2^n}{l_e^n \kappa^2} \langle f_n(\theta) K^2 \rangle v_{\lambda}^{n-4} T^{4-n}, \quad (14)$$

where $\langle f_n(\theta) K^2 \rangle$ is the effective piezo coupling. For graphene the electron-phonon coupling is dominated by deformation potential coupling [17] and vector potential coupling [18] ($G_{Lp}^{VP}(T)$) giving $G_{Lp}(T) = G_{Lp}^{DP}(T) + G_{Lp}^{VP}(T)$. For these both contributions we will use directly the results of Ref. [18].

III. RESULTS AND DISCUSSION

In this section, we calculate the interlayer thermal conductance G_{12} of selected semiconductor and graphene bilayer systems at the ballistic and diffusive limit and discuss possible experimental configurations to investigate G_{12} . Interlayer thermal conductance will be compared to electron-phonon thermal conductance G_{Lp} . Diffusive G_{12} is considered at larger interlayer separation than the ballistic one in order to assure that the diffusive response formula [Eq. (10)] is valid and condition $k_F l_e > 1$ is fulfilled.

A. Calculations for different bilayers

Figure 2 shows $G_{12}(T)$ obtained numerically from Eqs. (7) and (8) in the case of symmetric high mobility (ballistic) GaAs bilayer[3] [depicted in Fig. 1(c)] with single layer electron density $n = 10^{15} \text{ m}^{-2}$ and $d = 20 \text{ nm}$. Asymptotic limit formula of Eq. (11) is also plotted. In the phonon contribution we have $\sum_{\lambda} \langle \sin \theta \Xi^2 \rangle v_{\lambda}^{-6} = \frac{1}{4} \pi \Xi_d^2 v_L^{-6}$, where $\Xi_d = 10 \text{ eV}$ is the dilatational deformation potential constant, and $\sum_{\lambda} \langle \sin \theta K^2 \rangle v_{\lambda}^{-4} = \left(\frac{e}{\epsilon_b}\right)^2 e_{14}^2 \pi \left(\frac{89}{1024} v_L^{-4} + \frac{107}{1024} v_T^{-4}\right)$, where $e_{14} = -0.16 \text{ C/N}$ is the only non-zero element of the piezotensor. Other parameters can be found from Ref. [19]. Equations (13) and (14) are plotted as symbols in Fig. 2 in the ballistic limit of electron-phonon coupling. Below few Kelvin piezoelectric coupling fully dominates and as a result the temperature regime where $G_{Lp} < G_{12}$ is pushed towards relatively low, but experimentally achievable, temperatures. The crossover occurs at $T \sim 140 \text{ mK}$.

For silicon based bilayer [see Ref. [20] and Fig. 1(d)] we consider both ballistic and diffusive limits at electron density $n = 5 \times 10^{15} \text{ m}^{-2}$. Parameters for Si can be found from Ref. [19]. The curves in Fig. 3 are calculated for symmetric high (low) mobility Si bilayer system with mobility $\mu = 2.5$ (0.2) m^2/Vs , mean-free path $l_e = 200$ (16) nm and layer distance $d = 20$ (200) nm. For the high mobility device we have used the ballistic limit response [Eq. (8)] and for the low mobility one the diffusive response [Eq. (10)]. Silicon is not piezoelectric so for G_{Lp} we need to consider only G_{Lp}^{DP} . Due finite electron mean free path (even for the high mobility device) we will include ballistic and diffusive limits of G_{Lp}^{DP} . For simplicity we plot G_{Lp}^{DP} so that it changes abruptly from diffusive to ballistic formula [note that Eq. (13) is not valid close to $q_{\lambda T} l_e = 1$]. For Si 2DEG we have $\sum_{\lambda} \langle \sin \theta \Xi^2 \rangle v_{\lambda}^{-6} = \frac{1}{32} \pi (4 \Xi_d \Xi_u + 8 \Xi_d^2 + \Xi_u^2) v_L^{-6} + \frac{1}{32} \pi \Xi_u^2 v_T^{-6}$ and $\sum_{\lambda} \langle \Xi^2 \rangle v_{\lambda}^{-6} = \left(\frac{2}{3} \Xi_d \Xi_u + \Xi_d^2 + \frac{1}{5} \Xi_u^2\right) v_L^{-6} + \frac{2}{15} \Xi_u^2 v_T^{-6}$, where Ξ_u is the uniaxial deformation potential constant. We use the typical values $\Xi_{d(u)} = -11.7(9.0) \text{ eV}$. For the high and low mobility Si systems the crossover temperature where $G_{12} = G_{Lp}$ is 660 mK and 1.4 K, respectively. Even though we have set d an order of magnitude larger for the diffusive device, still the crossover occurs at higher temperature, which is the signature of the enhancement of fluctuations/dissipation and, thereby, interlayer coupling due to disorder. Note that deformation potential electron-phonon coupling is also enhanced due to disorder.

Next we consider graphene bilayer[4] that is depicted in Fig. 1(e). The curves in Fig. 4 are calculated for symmetric high (low) mobility device with mobility $\mu = 1.59$ (0.17) m^2/Vs , mean-free path $l_e = 10 \mu\text{m}$ (20 nm), layer distance $d = 20$ (200) nm and electron density $n = 10 \times 10^{15} \text{ m}^{-2}$. We have used $v_F = 10^6 \text{ m/s}$ and assumed AlO dielectric between the layers. As above, for the high mobility and for low mobility device we use ballistic and diffusive response

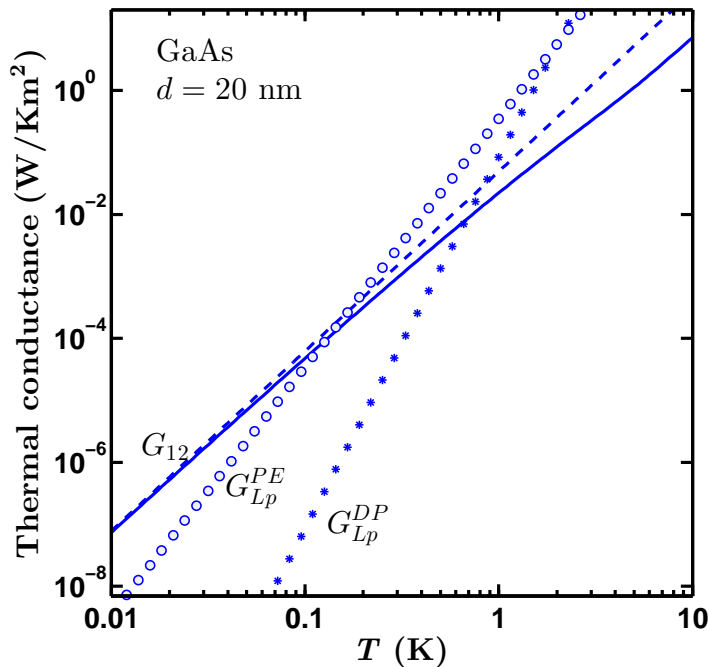


FIG. 2. (color online) The interlayer thermal conductance (G_{12}) and deformation potential (G_{Lp}^{DP}) and piezoelectric (G_{Lp}^{PE}) electron-phonon thermal conductance at the ballistic limit for GaAs bilayer system with electron density $n = 10^{15} \text{ m}^{-2}$. Solid curve is the result from numerical integration using the ballistic response function. Dashed curve obtained using Eq. (11).

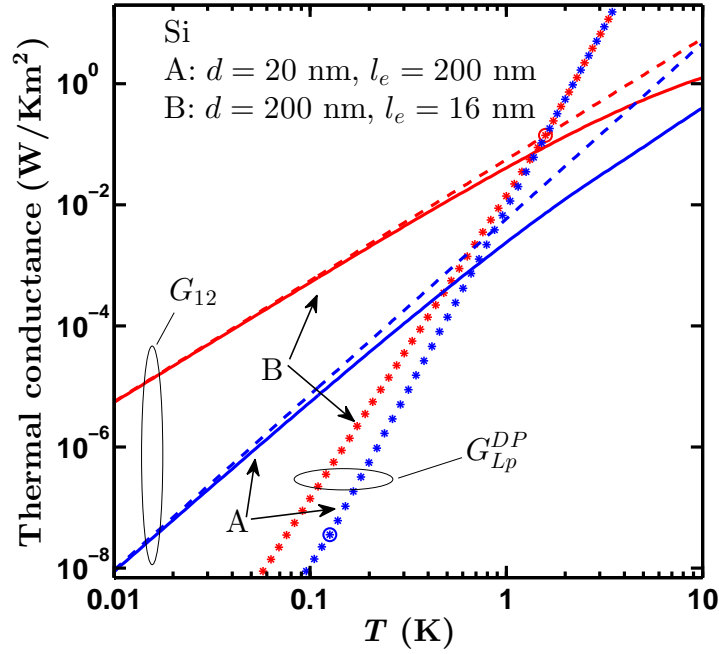


FIG. 3. (color online) The interlayer thermal conductance (G_{12}) and deformation potential (G_{Lp}^{DP}) electron-phonon thermal conductance for two Si bilayer devices with $n = 5 \times 10^{15} \text{ m}^{-2}$. For device A (B) solid curves are results from numerical integration using the ballistic (diffusive) susceptibility and dashed curves are obtained from the approximation formula of Eq. (11) (Eq. (12)). The circle marks the crossover where electron-phonon coupling changes from ballistic to diffusive.

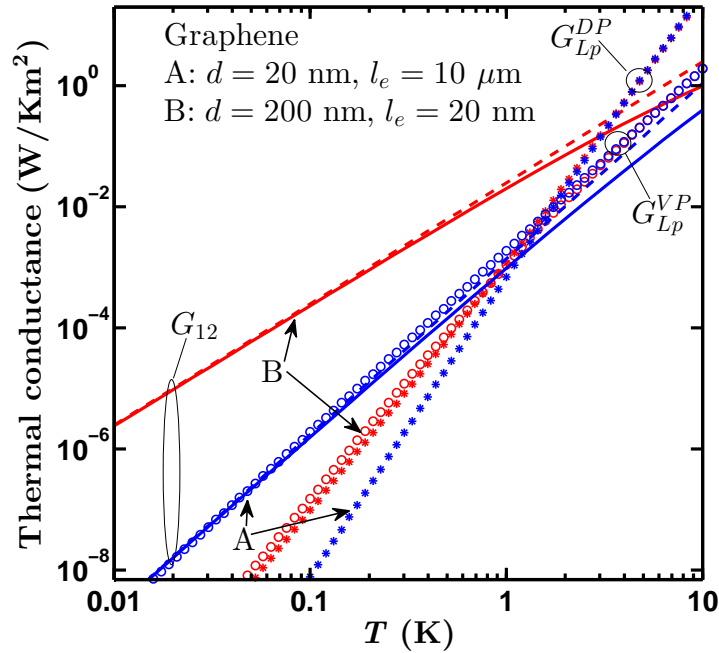


FIG. 4. (color online) The interlayer thermal conductance (G_{12}), deformation potential (G_{Lp}^{DP}) and vector potential (G_{Lp}^{VP}) electron-phonon thermal conductance for two graphene bilayer devices with $n = 1 \times 10^{16} \text{ m}^{-2}$. G_{Lp}^{DP} and G_{Lp}^{VP} are from Ref. [18]. For device A (B) solid curves are results from numerical integration using the ballistic (diffusive) susceptibility and dashed curves are obtained from the approximation formula of Eq. (11) (Eq. (12)).

functions, respectively. Screened deformation potential and vector potential electron-phonon contributions are plotted in Fig. 4 as symbols. For high mobility graphene G_{LP}^{VP} dominates at the lowest temperatures and the cross-over where $G_{12} = G_{LP}$ occurs at relatively low temperature of $T = 40$ mK. The disorder enhancement of the interlayer heat transfer pushes the threshold for low mobility graphene to $T = 3.0$ K. Note that the vector potential electron-phonon coupling is decreased with the disorder in contrast to deformation potential coupling.

Another widely explored semiconductor bilayer carrier system, which can be realized using compound semiconductors[21] or Si[22, 23], is the electron-hole bilayer. The complexity of the valence band makes this system more difficult to analyze theoretically. We will not present G_{12} for such system here explicitly, but it should behave in similar fashion as its electron-electron counter part. However, one thing that may differ drastically from electron-electron bilayer system is the carrier-phonon coupling. Due to asymmetry in the deformation potential coupling between the different layers the carrier-phonon coupling can be unscreened and as a result G_{LP} can be strongly enhanced at low temperatures. [15] The enhancement factor depends on the details of the system, but in many cases it is of the order of $(\kappa/q\lambda T)^2$, which suggests that for semiconductor electron-hole bilayers G_{LP} can dominate over G_{12} even down to very low temperatures. Note that also in symmetric electron bilayers G_{LP} can be affected by the presence of another carrier system in non-trivial way, but significant enhancement is not expected[15].

B. Possible experimental realizations

The interlayer heat transfer can be investigated experimentally by varying the input powers P_L while measuring the electron temperatures T_L [see Fig. 1(b)]. Uniform input power follows, for example, from Ohmic heating. This technique has been broadly utilized in the electron-phonon coupling measurements. Indeed, the electron-phonon contributions G_{LP} can be investigated independently from G_{12} at balanced input power that gives $T_1 = T_2$. In the case of semiconductor bilayer the other layer can be also depleted to get a handle on G_{LP} . Note that the Ohmic heating technique has been utilized also in the investigation of coupling of Johnson-Nyquist noise heating between two resistors at different temperature[24], which is conceptually very close to the case presented here.

It is not necessarily trivial to measure electron temperature of the individual layers. For example, quantum corrections of resistivity and Shubnikov- de Haas oscillations, that have been used as electron thermometer, can be affected by the other layer in a complicated way. More local temperature probes based, e.g., on quantum point contacts and quantum dots have also been investigated.[25–27] Noise thermometry provides an attractive way to probe electron temperature. It has been recently used for single layer graphene [28] and could be adopted in investigations of G_{12} .

Interlayer heat transfer can also be investigated in more indirect way by coupling the individual layers to metallic electrodes, to which the input power is fed and where temperature is sensed. As metals have quite large electron-phonon coupling the volume of the metallic islands should be sufficiently small in order not to hide G_{12} . Especially in the case of Si, doped contact regions can serve as the metallic islands. This is attractive approach as the electron-phonon coupling in doped semiconductors can be relative weak so that G_{12} still dominates. The sign of P_L can be also reversed, which is equivalent to cooling. This can be achieved by quantum dots [26] or semiconductor-superconductor contacts [29].

As G_{12} (and G_{LP}) depends on the electron densities and on the interlayer density balance it is desirable to adjust the layer densities by external gates. In general, G_{12} could be used as a gate voltage controlled thermalization path (thermal switch). However, it is important to note (as already pointed out in Ref.[15]) that similar near-field thermal coupling to G_{12} can exist between the 2D carriers and the external gate electrodes.

IV. SUMMARY AND CONCLUSIONS

In summary, a near-field heat transfer effect due to interlayer interaction in bilayer carrier systems was investigated. By using perturbation theory and fluctuation-dissipation relations we derived a general expression of near-field interlayer energy transfer rate [Eq. (6)] and thermal conductance [Eq. (7)]. Our formulation can be applied, for example, to semiconductor and graphene based bilayers. We presented analytical approximation formulas and detailed calculations of interlayer heat transfer due to screened Coulomb interaction for GaAs, Si and graphene based bilayers. It was shown that remarkably the interlayer heat transfer can dominate over the electron-phonon coupling to the thermal bath below a crossover temperature that depends on the system parameters. We found a crossover temperature of 140 mK (660 mK) for ballistic GaAs (Si) bilayer with $d = 20$ nm layer distance and carrier density $n = 10^{15} \text{ m}^{-2}$ ($5 \times 10^{15} \text{ m}^{-2}$). Strong vector potential electron-phonon coupling in ballistic graphene results in low crossover temperature of 40 mK ($n = 10 \times 10^{15} \text{ m}^{-2}$). Interlayer heat transfer is enhanced by disorder and for low mobility Si (graphene) bilayer with $d = 200$ nm the crossover occurs already at ~ 1.4 K (3.0 K). The crossover temperatures reported here can be

accessed by standard experimental equipment and we introduced possible experimental configurations to investigate the interlayer heat transfer.

Finally, we note that by lowering the electron densities and/or by increasing the temperature plasmons and virtual phonons may start to play a role in the interlayer interaction. These excitations are known to enhance the bilayer drag effect [30, 31] and the enhancement should also be observable in the interlayer heat transfer. In a very dilute and strongly interacting systems enhancement of drag, that cannot be explained with plasmons or virtual phonons, has also been observed.[32] Therefore, depending on the system parameters the crossover temperature, below which the interlayer heat transfer starts to dominate over the electron-phonon coupling to the thermal bath, can be significantly higher than the ones given in this work. Studies of plasmonic effects, virtual phonon excitations, dilute carrier regime and elevated temperatures are left for future investigations. At elevated temperatures the effect described in this paper can also be of relevance for inter-flake heat transfer in thermal interface materials fabricated from graphene composites.[33] The concepts presented in this work can be extended to coupled one-dimensional carrier systems.

ACKNOWLEDGMENTS

The authors want to acknowledge useful discussions with P.-O. Chapuis, K. Flensberg and D. Gunnarsson. This work has been partially funded by the Academy of Finland through grant 252598 and by EU through project 256959 NANOPOWER.

-
- [1] A. G. Rojo, J. Phys. Condens. Matter **11**, R31 (1999).
 - [2] K. Das Gupta, A. F. Croxall, J. Waldie, C. A. Nicoll, H. E. Beere, I. Farrer, D. A. Ritchie, and M. Pepper, Advances in Condensed Matter Physics **2011**, 727958 (2011).
 - [3] T. J. Gramila, J. P. Eisenstein, A. H. MacDonald, L. N. Pfeiffer, and K. W. West, Phys.Rev.Lett. **66**, 1216 (1991).
 - [4] S. Kim, I. Jo, J. Nah, Z. Yao, S. K. Banerjee, and E. Tutuc, Phys. Rev. B **83**, 161401 (2011).
 - [5] J. B. Pendry, J. Phys.: Condens. Matter **11**, 6621 (1999).
 - [6] K. Joulain, J.-P. Mulet, F. Marquier, R. Carminati, and J.-J. Greffet, Surface Science Reports **57**, 59 (2005).
 - [7] A. I. Volokitin and B. N. J. Persson, Rev. Mod. Phys. **79**, 1291 (2007).
 - [8] M. Prunnila and J. Meltaus, Phys. Rev. Lett. **105**, 125501 (2010).
 - [9] I. Altfeder, A. A. Voevodin, and A. K. Roy, Phys. Rev. Lett. **105**, 166101 (2010).
 - [10] K. Flensberg, B. Hu, A. Jauho, and J. M. Kinaret, Phys. Rev. B **52**, 14761 (1995).
 - [11] R. Kubo, Rep. Prog. Phys. **29**, 255 (1966).
 - [12] F. Stern, Phys. Rev. Lett. **18**, 546 (1967).
 - [13] E. H. Hwang and S. D. Sarma, Phys. Rev. B **75**, 205418 (2007).
 - [14] P. J. Price, J. Appl. Phys. **53**, 6863 (1982).
 - [15] M. Prunnila, Phys. Rev. B **75**, 165322 (2007).
 - [16] D. V. Khveshchenko and M. Y. Reizer, Phys. Rev. Lett. **78**, 3531 (1997).
 - [17] J. K. Viljas and T. T. Heikkil, Phys. Rev. B **81**, 245404 (2010).
 - [18] W. Chen and A. A. Clerk (2012), arXiv:1207.2730.
 - [19] O. Madelung, *Semiconductors: Data Handbook* (Springer, 2004).
 - [20] K. Takashina, Y. Hirayama, A. Fujiwara, S. Horiguchi, and Y. Takahashi, Physica E **22**, 72 (2004).
 - [21] M. Prunnila, J. Ahopelto, and H. Sakaki, Phys. Stat. Sol.(a) **202**, 970 (2005).
 - [22] U. Sivan, P. M. Solomon, and H. Shtrikman, Phys.Rev.Lett. **68**, 1196 (1992).
 - [23] M. Prunnila, S. J. Laakso, J. M. Kivioja, and J. Ahopelto, Appl. Phys. Lett. **93**, 112113 (2008).
 - [24] K. Takashina, K. Nishiguchi, Y. Ono, A. Fujiwara, T. Fujisawa, Y. Hirayama, and K. Muraki, Appl. Phys. Lett. **94**, 142104 (2009).
 - [25] M. Meschke, W. Guichard, and J. P. Pekola, Nature **44**, 187 (2006).
 - [26] N. J. Appleyard, J. T. Nicholls, M. Y. Simmons, W. R. Tribe, and M. Pepper, Phys. Rev. Lett. **81**, 3491 (1998).
 - [27] J. R. Prance, C. G. Smith, J. P. Griffiths, S. J. Chorley, D. Anderson, G. A. C. Jones, I. Farrer, and D. A. Ritchie, Phys. Rev. Lett. **102**, 146602 (2009).
 - [28] S. Gasparinetti, M. J. Martinez-Perez, S. de Franceschi, J. P. Pekola, and F. Giazotto, Applied Physics Letters **100**, 253502 (2012).
 - [29] K. Fong and K. Schwab (2012), arXiv:1202.5737.
 - [30] A. M. Savin, M. Prunnila, P. P. Kivinen, J. P. Pekola, J. Ahopelto, and A. J. Manninen, Appl. Phys. Lett. **79**, 1471 (2001).
 - [31] K. Flensberg and B. Y.-K. Hu, Phys. Rev. Lett. **73**, 3572 (1994).
 - [32] M. C. Bønsager, K. Flensberg, B. Yu-Kuang Hu, and A. H. MacDonald, Phys. Rev. B **57**, 7085 (1998).
 - [33] R. Pillarisetty, H. Noh, D. C. Tsui, E. P. De Poortere, E. Tutuc, and M. Shayegan, Phys. Rev. Lett. **89**, 016805 (2002).